# Influence of gouge thickness on permeability of macro-fractured basalt

AUTHOR(S):

Wang, G.; Mitchell, T. M.; Meredith, P. G.; Nara, Y.; Wu, Z.

CITATION:

Wang, G. ...[et al]. Influence of gouge thickness on permeability of macro-fractured basalt. Journal of Geophysical Research: Solid Earth 2016, 121(12): 8472-8487

ISSUE DATE:

2016-12

AGU PUBLICATIONS
JGR
Journal of Geophysical Research: Solid Earth

RESEARCH ARTICLE
10.1002/2016JB013363

Special Section:
Rock Physics of the Upper Crust

# Influence of gouge thickness and grain size on permeability of macrofractured basalt

G. Wang[1,2], T. M. Mitchell[2], P. G. Meredith[2], Y. Nara[3], and Z. Wu[1]

[1]School of Geosciences, China University of Petroleum, Qingdao, China, [2]Department of Earth Sciences, University College London, London, UK, [3]Graduate School of Engineering, Kyoto University, Kyoto, Japan

**Key Points:**
- Fracture permeability is dramatically reduced in the presence of fault gouge
- Variation of gouge thickness and grain size can lead to large changes in fracture permeability
- Pressure cycling causes reduction in fracture permeability due to grain packing and/or comminution of gouge particles

**Correspondence to:**
G. Wang,
guangzengwang@gmail.com

**Citation:**
Wang, G., T. M. Mitchell, P. G. Meredith, Y. Nara, and Z. Wu (2016), Influence of gouge thickness and grain size on permeability of macrofractured basalt, *J. Geophys. Res. Solid Earth*, *121*, 8472–8487, doi:10.1002/2016JB013363.

Received 18 JUL 2016
Accepted 1 DEC 2016
Accepted article online 6 DEC 2016
Published online 14 DEC 2016



**Abstract** Fractures allow crystalline rocks to store and transport fluids, but fracture permeability can also be influenced significantly by the existence or absence of gouge and by stress history. To investigate these issues, we measured the water permeability of macrofractured basalt samples unfilled or infilled with gouge of different grain sizes and thicknesses as a function of hydrostatic stress and also under cyclic stress conditions. In all experiments, permeability decreased with increasing effective pressure, but unfilled fractures exhibited a much greater decrease than gouge-filled fractures. Macrofractures filled with fine-grained gouge had the lowest permeabilities and exhibited the smallest change with pressure. By contrast, the permeability changed significantly more in fractures filled with coarser-grained gouge. During cyclic pressurization, permeability decreased with increasing cycle number until reaching a minimum value after a certain number of cycles. Permeability reduction in unfilled fractures is accommodated by both elastic and inelastic deformation of surface asperities, while measurements of the particle size distribution and compaction in gouge-filled fractures indicate only inelastic compaction. In fine-grained gouge this is accommodated by grain rearrangement, while in coarser-grained gouge it is the result of both grain rearrangement and comminution. Overall, sample permeability is dominated by the gouge permeability, which decreases with increasing thickness and is also sensitive to the grain size and its distribution. Our results imply that there is a crossover depth in the crust below which the permeability of well-mated fractures (e.g., joints) becomes lower than that of gouge-filled fractures (e.g., shear faults).

## 1. Introduction

Permeability is the key parameter in predicting the flow of fluids in the subsurface, such as water, oil, or gas, especially flow within percolating fracture networks [*Gueguen et al.*, 1997; *Min et al.*, 2004; *Nara et al.*, 2011; *Walsh*, 1981]. However, the flow properties of these fractures can be changed significantly by the presence of fault products contained within them, such as fault gouge. Such products can provide potential barriers to fluid flow, with major implications for fault mechanics [*Anthony and Marone*, 2005; *Deming*, 1994; *Faulkner and Rutter*, 1998, 2000; *Lang and Anthony*, 2004; *Nara et al.*, 2013; *Rutter et al.*, 1986; *Watts*, 1987]. It is therefore important to investigate how fault gouge influences fluid flow in fractures as a function of elevated normal stress, since this has important implications for both natural hazards, such as earthquakes, and geoengineering issues, such as aquifers, hydrocarbon reservoirs, and repositories for hazardous waste [*Berkowitz*, 2002; *Ma*, 2015; *Nara et al.*, 2011].

Numerous laboratory studies have been carried out to investigate the effect of hydrostatic or differential stress on the transport properties of fractures containing either artificial or natural fault gouge of different mineral compositions, and a number of general conclusions have been reached: (1) an inverse relationship exists between permeability and effective normal stress, regardless of whether any shear stress is applied or not [*Crawford et al.*, 2008; *Faulkner and Rutter*, 1998, 2000; *Morrow et al.*, 1981, 1984; *Nara et al.*, 2013; *Screaton et al.*, 1990; *Uehara and Shimamoto*, 2004; *Zhang and Tullis*, 1998; *Zhang et al.*, 1999, 2001]; (2) the formation of microstructures, such as *P*, *R*, or *Y* shears, within the gouge during shearing involves grain crushing and porosity reduction that can induce permeability anisotropy, with permeability parallel to the fault commonly several orders of magnitude higher than that perpendicular to it [*Aydin*, 1978; *Bied et al.*, 2002; *Faulkner and Rutter*, 1998, 2000; *Zhang and Tullis*, 1998; *Zhang et al.*, 1999, 2001]; and (3) the presence of water, possibly the most common geofluid, can facilitate fluid-rock reactions, due to its polarized nature and the presence of free charge on mineral surfaces, which can lower the permeability significantly [*Faulkner and Rutter*, 2000]. Furthermore, *Morrow et al.* [1984] found that mineral composition and grain size were also important influences on gouge permeability, with montmorillonite-rich and finer grained nonclay

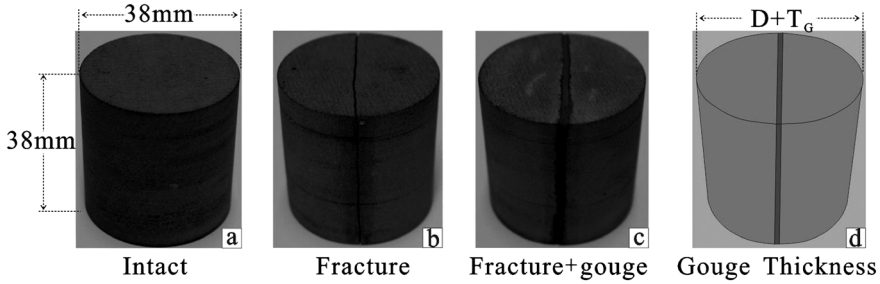


**Figure 1.** Seljadalur basalt samples used in our experiments: (a) intact sample, (b) sample with an axial macrofracture, (c) sample filled with artificial gouge, and (d) schematic diagram of gouge thickness measurement.

gouges having the lowest permeabilities, while serpentine-rich and coarser grained nonclay gouges had the highest permeability. *Faulkner and Rutter* [2000] reported that pressure cycling also reduced the permeability of clay-bearing gouge but that a constant minimum value was eventually reached after multiple pressure cycles.

However, much of this previous work has focused on gouge of either a fixed grain size or a narrow grain-size fraction. Few studies have investigated the effect of gouge thickness on fracture permeability, even though this is considered to be an important factor influencing the sealing capacity of faults [*Deming*, 1994; *Watts*, 1987]. Furthermore, in spite of the limited work of *Morrow et al.* [1984] and *Faulkner and Rutter* [2000], there remain many unanswered questions about the role that particle size distribution, gouge thickness, and pressure cycling play in influencing fracture permeability. In this study, we have therefore investigated systematically the permeability evolution within macrofractures in basalt, either unfilled or filled with synthetic fault gouge of varying particle size distribution and thickness. We also compare the permeability evolution during a single hydrostatic pressure cycle and multiple pressure cycles.

## 2. Experimental Materials and Methodology

### 2.1. Sample Material and Sample Preparation

To study the effect of gouge on fluid flow through macrofractures, it was important to minimize the influence of the matrix permeability. We therefore selected a rock with a very low matrix permeability, namely, Seljadalur basalt (SB) previously used by *Nara et al.* [2011] and *Nara et al.*, 2013. SB has no visible preexisting microfractures or macrofractures, a density of 2900 kg/m$^3$ $\pm$ 10 kg/m$^3$, a porosity of around 4%, and, importantly, a very low permeability of around $10^{-20}$ m$^2$. It is an intrusive, tholeiitic basalt from southeast Iceland [*Eccles et al.*, 2005], and mainly composed of an intergranular matrix of plagioclase, granular pyroxene, and iron oxides. Partially oriented plagioclase microphenocrysts are found along with a rare abundance of augite, olivine, and an interstitial glass phase.

Cylindrical core samples, 38 mm in diameter and 38 mm in length, were first prepared from the same batch of SB as that used in *Nara et al.* [2011] and *Nara et al.*, 2013 (Figure 1a). We then used the Brazil disk technique to introduce axial macrofractures across the diameter of previously intact samples. During this process, three layers of 0.3 mm thick adhesive tape were wrapped around the circumference of each sample as this minimized the tendency for multiple fractures to be generated. Only samples with a single, diametral macrofracture and no other visible fractures were chosen for our permeability experiments (Figure 1b).

Natural fault gouges contain a distribution of grain sizes below some upper limit [*Sammis et al.*, 1986]. Progressive evolution of gouge generally produces material with increasingly finer particle sizes before reaching a comminution limit at which grain size reduction ceases [*An and Sammis*, 1994; *Cladouhos*, 1999; *Kendall*, 1978; *Michibayashi*, 1996]. To study the effect of fracture-fill on permeability, we crushed and milled pieces of SB to create a series of synthetic fault gouges with different grain size distributions, with longer milling times producing finer gouges. We then used sieves with mesh sizes ranging from 63 μm to 500 μm to sort the milled material into the desired size fractions of ≤63 μm, ≤108 μm, ≤125 μm, ≤250 μm, and ≤500 μm.

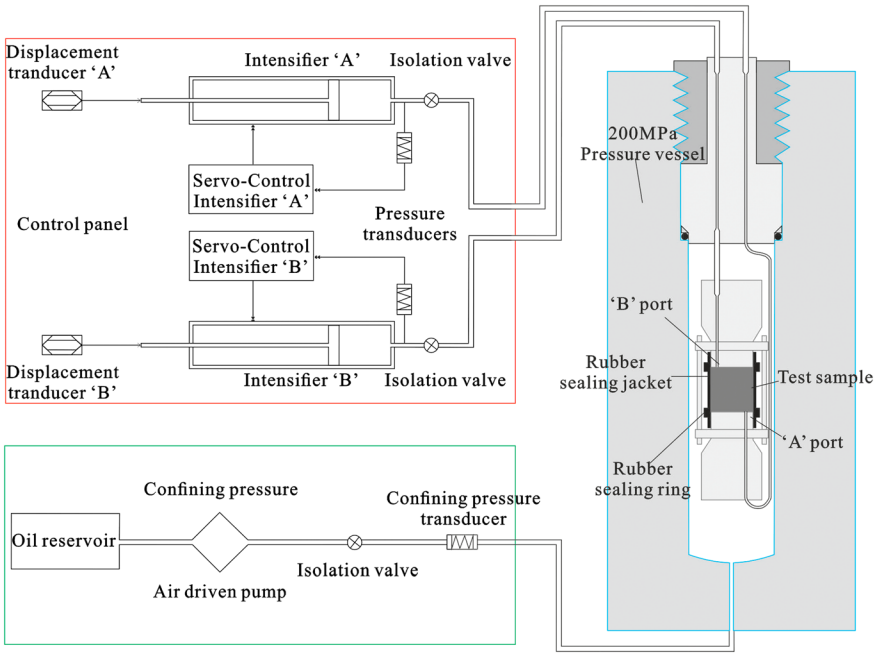


**Figure 2.** Schematic diagram of the permeameter used for all permeability measurements.

To facilitate sample preparation, we added one drop of distilled water for every 10 g of the synthetic gouge, which ensured wetting but without saturation. A given thickness of the wetted gouge was then applied to one half of the previously macrofractured sample and the other half sample placed on top to produce a "sandwich" sample (Figure 1c). The sandwich sample was then placed within an elastomer jacket which holds the sample together by providing a small initial compressive load. Pore fluid distribution disks were placed over each end of the sample and within the elastomer jacket to allow water flow but to prevent any loss of gouge material. By introducing a layer of gouge, the sample diameter perpendicular to the fracture is increased by the layer thickness as shown in Figure 1d, where $D$ is the initial sample diameter (38 mm) and $T_G$ is the thickness of the gouge layer. The overall thickness ($D + T_g$) was measured using a Vernier caliper before the sandwich sample was placed in the jacket, with the error in measurement of the gouge layer thickness being less than 0.01 mm. Finally, the complete sample assembly was placed in a hydrostatic permeameter for testing.

## 2.2. Methodology

### 2.2.1. Permeability Measurement

All permeability measurements were made in a servo-controlled permeameter using the steady state flow method, as shown schematically in Figure 2. The system utilizes a 200 MPa hydrostatic pressure vessel connected to two 70 MPa servo-controlled pore fluid intensifiers. The jacketed sample assembly is placed inside the pressure vessel and fixed between two stainless steel end caps. A preset pore fluid pressure gradient ensures fluid flow through the sample. In all experiments, deionized water was used as the pore fluid, and silicone oil was used as the confining pressure fluid. To eliminate the influence of temperature-induced pressure fluctuations, the permeameter is located in a temperature-controlled laboratory (18°C). During all permeability measurements of this study the mean pore pressure was held at 4 MPa with a 1 MPa pore pressure difference set between the upstream and downstream intensifiers. We calculated effective pressure ($P_{eff}$) from the simple effective pressure law: $P_{eff} = P_c - \alpha . P_f$ where $P_c$ is the applied confining pressure, $P_f$ is the mean pore fluid pressure, and the poroelastic constant $\alpha = 1$ [*Morrow et al.*, 1986]. The confining pressure was not servo controlled but was set to the desired value at the start of each experimental step and maintained constant throughout that step. In this study, the effective pressure was varied from 5 MPa to 60 MPa by stepwise changes in the confining pressure while maintaining a constant pore fluid pressure. The resolutions of $P_c$ and $P_f$ are both 0.01 MPa. Following each change in pressure, the system was held at that constant pressure until steady state flow was achieved before making any measurements (the minimum hold time

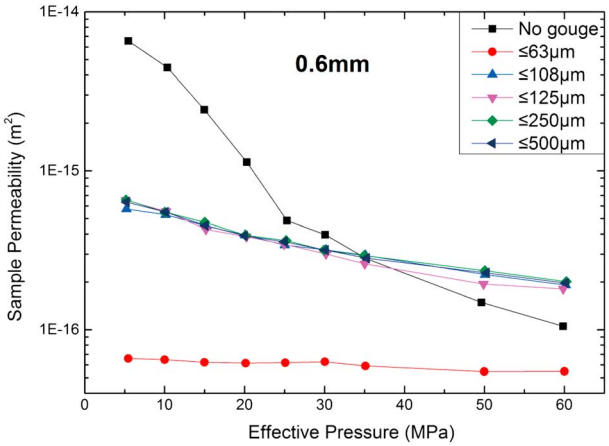


**Figure 3.** Permeability of macrofractured sample with no gouge and with gouge layers of the same thickness (0.6 mm) but different grain sizes of ≤63, ≤108, ≤125, ≤250, and ≤500 μm, under elevated effective pressure.

being 30 min). Sample permeability ***k*** was calculated from the volumetric flow rate of the pore fluid ***Q***, the fluid viscosity $\mu$, the cross-sectional area of the sample ***A***, and the pressure difference $\Delta P$ across the sample of length ***L***, by direct application of Darcy's law:

$$k = -(Q.L.\mu)/(A.\Delta P) \quad (1)$$

All permeability data are reported as "sample" permeabilities. That is, the value for ***A*** in equation (1) is the total cross-sectional area of the sample. For samples with unfilled fractures (no gouge) this is simply the circular cross-sectional area of the core, but for samples with gouge-filled fractures it is this circular cross section plus the cross-sectional area of the gouge layer. To reduce the computation errors and take the compaction of gouge into consideration during experiments, the thickness of the gouge layer used to calculate the cross-sectional area in equation (1) is the mean of the initial gouge thickness and the final gouge thickness measured after the end of each permeability experiment (i.e., after 1 or *N* pressure cycles).

#### 2.2.2. Particle Size Analysis

Analysis of the particle size distribution (PSD) of our synthetic gouges was determined using a Malvern Instruments Ltd., Mastersizer APA 2000 laser diffraction apparatus, using the Mie theory of light scattering. Particle sizes are reported as volume equivalent sphere diameters. To improve the dispersion of grains within the gouge, the apparatus is equipped with a Hydro 2000S-AWA2001 dispersion unit. To ensure measurement accuracy, all PSD measurements in this study were performed in triplicate at a constant temperature of 18°C.

We did a number of repeat tests for every individual test condition. The results (changes of permeability, PSD and thickness of gouge) were very reproducible, so we only present the results from one test for each test condition here.

## 3. Experimental Results

### 3.1. Permeability Data

#### 3.1.1. Effect of Gouge Grain Size

Initial permeability measurements were made on unfilled (no gouge) macrofractured samples at effective pressures from 5 MPa to 60 MPa as a baseline. Measurements were then repeated on the same samples but filled with 0.6 mm thick layers of preprepared synthetic fault gouge of different grain sizes. The changes in permeability as functions of increasing effective pressure and gouge grain size are shown in Figure 3.

As expected, the presence of a macrofracture increases the sample permeability significantly for all cases, whether unfilled or filled with a gouge layer, from about $10^{-20}$ m$^2$ for an intact sample [*Nara et al*., 2011] to within the range of $10^{-17}$–$10^{-14}$ m$^2$. Permeability also decreases with increasing effective pressure in all cases, with the largest decrease seen for the unfilled sample, which had the highest starting permeability.

A nonlinear relationship between permeability and effective pressure was observed for the unfilled sample in Figure 3, with permeability dropping by a factor of 15 over the pressure range from 5 to 25 MPa followed by a much more gradual decrease by a further factor of 5 over the pressure range from 25 to 60 MPa. By contrast, all the samples with gouge-filled fractures exhibited a quasi-linear decrease in permeability with increasing effective pressure, which is consistent with the observations of *Zhang et al*. [2001] and *Crawford et al*. [2008]. In particular, the sample with its fracture filled with the finest gouge (≤63 μm) has the lowest permeability, which decreases by only about 20% from around $7 \times 10^{-17}$ m$^2$ to around $5.5 \times 10^{-17}$ m$^2$ over the full pressure range and which is also lower than the permeability of the unfilled sample at all effective pressures. In between these end-member cases, the permeability of samples with macrofractures filled with gouges of

particle sizes ≤108, ≤125, ≤250, and ≤500 μm behave remarkably similarly. Their absolute permeabilties are extremely similar, and their variation with effective pressure is almost identical; decreasing by about half an order of magnitude from $7\times10^{-16}$ to $2\times10^{-16}$ m$^2$ over the full pressure range. We also note that the permeability of all these latter samples is lower than for the unfilled fracture up to 35 MPa but higher at all effective pressures above this value. The data of Figure 3 clearly show a significant difference in behavior between the finest grain size gouge and all the other gouges, which agrees with the observations of *Krumbein and Aberdeen* [1937] that the behavior of gouge changes significantly at a critical grain size of 63 μm. It seems likely that the presence of particles with sizes > 63 μm act to prop open the fracture and hence increase its permeability. Such a process would also explain why the permeability of the samples with coarser-grained gouges is higher than the unfilled fracture at the higher effective pressures.

As noted earlier, all permeability data reported here are sample permeabilities, with the value for $A$ in equation (1) being the total cross-sectional area of the fractured cylindrical sample plus the cross-sectional area of the gouge layer (when present). However, the data of Figure 3 show clearly that the permeabilities of all gouge-filled samples are multiple orders of magnitude higher than that of the intact, unfractured basalt (around $10^{-20}$ m$^2$) [*Nara et al*., 2011]. There is therefore negligible flow through the matrix, and we are essentially measuring the permeability of the gouge layer. The relationship between sample permeability and "gouge" permeability is discussed in detail later in section 4.1.3.

#### 3.1.2. Effect of Gouge Thickness

Several authors have reported that gouge thickness is an important factor influencing fluid flow in fractured rocks [*Deming*, 1994; *Watts*, 1987]. We have therefore investigated the effect of gouge thickness on permeability using subsets of our gouges with grain sizes of ≤63 μm and ≤250 μm. We used the same methodology to measure the permeability of samples with gouge thickness from 0.2 mm to 1.9 mm for the ≤63 μm gouge and from 0.3 mm to 2.0 mm for the ≤250 μm gouge, respectively. The results are presented in Figure 4.

For the fine-grained gouge, the results show that permeability changes very little with increasing gouge thickness, changing by only about 50% over the whole effective pressure range studied. Also, there does not appear to be any consistent variation with thickness. However, the permeability always remains lower than that of the unfilled fracture for all pressures and all thicknesses. By contrast, results for the coarser-grained gouge show that permeability increases consistently with increasing gouge thickness for all effective pressures. Furthermore, the change in permeability is larger than for the fine-grained gouge, with the permeability increasing by a factor of between 2 and 3 as gouge thickness is increased from 0.3 mm to 2.0 mm. These increases change the point at which the permeability of the gouge-filled fracture becomes higher than the unfilled fracture. For the thickest gouge layer (2.0 mm), the permeability of the gouge filled fracture becomes higher than that of the unfilled fracture at an effective pressure of around 25 MPa. This permeability crossover pressure increases with decreasing gouge thickness, until for the thinnest gouge layer (0.3 mm) the permeability of the gouge layer remains below that of the unfilled fracture at all pressures up to the maximum of 60 MPa. This observation supports our previous suggestion that the coarser-grained gouges act to prop open the fracture, with thicker gouges propping the crack open more and thus increasing its permeability.

#### 3.1.3. Effect of Pressure Cycling

Important rock properties affecting fluid flow, such as fracture opening and closure, are known to be dependent on stress history [*Bernabe*, 1987; *Hadley*, 1976; *Scholz and Koczynski*, 1979; *Zoback and Byerlee*, 1975]. A hysteresis phenomenon [*Scholz and Hickman*, 1983; *Wissler and Simmons*, 1985] has also been reported during permeability measurements on sandstone, granite [e.g., *Bernabe*, 1987; *Morrow et al*., 1986; *Wong*, 1990], and fault gouge [*Faulkner and Rutter*, 1998, 2000] during pressure cycling. We therefore investigated the effect of cyclic pressurization and depressurization on our macrofractured samples. Baseline permeability measurements were first made on a sample with an unfilled fracture. This was followed by measurements on samples with fractures filled with 0.6 mm thick layers of gouges with grain sizes of ≤63 μm, ≤125 μm, and ≤250 μm. All measurements were made at each value of effective pressure using the same protocol. Effective pressure was increased in 5 MPa steps from 5 MPa to 40 MPa and then in 10 MPa steps from 40 MPa to 60 MPa, with an exactly similar set of measurements made during depressurization in a reverse stepwise manner. Cycles of pressurization and depressurization were then repeated until the permeability reached steady state (i.e., no further changes were seen on subsequent cycles). The number of cycles required to reach steady state varied from 3 to 12 and depended on the characteristics of the gouge.

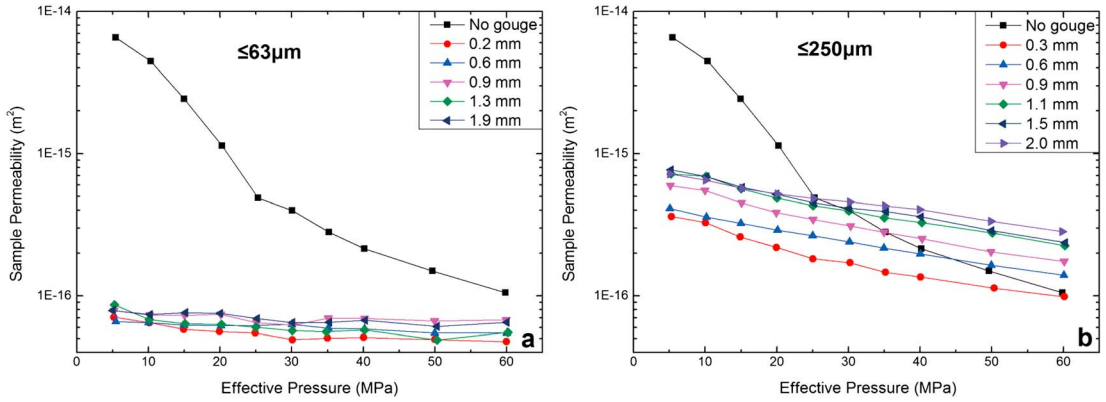


**Figure 4.** Permeability of samples filled with different gouge thicknesses under increasing effective pressure for gouge made of (a) ≤63 μm size particles and gouge made of (b) ≤250 μm size particles.

The results of our pressure cycling permeability measurements are shown in Figure 5. Here for clarity, we plot all the data from the first three cycles plus the data from the cycle where the permeability reached steady state. Figure 5a shows the evolution of permeability in an unfilled fracture during pressure cycling. As before, the permeability decreases rapidly as effective pressure is increased up to around 25 MPa and decreases at a much lower rate at higher pressures. The initial rapid decrease appears to be maintained in every cycle, but the rate of decrease at higher pressure decreases markedly with increasing cycle number. A large permeability hysteresis is observed on the first cycle, with the permeabilities during depressurization being much lower than during pressurization at the same effective pressure. The permeability does not recover its initial value on depressurization, so the observed hysteresis involves inelastic as well as elastic processes. However, the magnitude of the hysteresis is significantly reduced on each successive cycle, until eventually a purely elastic hysteresis loop is observed on the final cycle (12th in this case) with the permeability fully recovering its starting value for that cycle on depressurization. Overall, however, the steady state permeability on the 12th cycle is a factor of 6 lower than the initial value at 5 MPa and a factor of 2.5 lower at 60 MPa.

The permeability of samples with gouge-filled fractures also decreases during progressive pressure cycling, but much less than for the unfilled fracture. We also note that the permeability in these samples reach steady state over fewer cycles than for the unfilled fracture. The permeability of the sample with its fracture filled with the finest-grained gouge (≤63 μm) appears less sensitive to pressure cycling than those with the coarser-grained gouges (Figure 5b), exhibiting minimal hysteresis. Only a small overall reduction in permeability is observed, reaching steady state after only three cycles. By contrast, the samples with coarser ≤125 μm and ≤250 μm gouges require eight and nine cycles, respectively, to reach a steady state permeability (Figures 5c and 5d). Again, they exhibit a nearly linear change in permeability with change in effective pressure, both increasing and decreasing. They also show significant hysteresis during the first cycle, but very little during subsequent cycles. Overall, the permeability reduction between values on the first cycle and the steady state values varies between a factor of 2 and 4, somewhat higher than for the fine-grained gouge but much lower than for the unfilled fracture.

### 3.2. Gouge Thickness and Particle Size Distribution Analysis

Since our experiments are necessarily conducted inside a pressure vessel, it is not possible to directly observe the micromechanisms within the gouge material responsible for the observed differences in measured permeability. Thus, the links between our experimental results and the particle dynamics that are responsible for them, including particle rearrangement and fracture, must be inferred indirectly from the inelastic deformation of the gouge [*Amiri Hossaini et al.*, 2014], such as changes in gouge thickness and particle size distribution (PSD) before and after the tests [*Mair et al.*, 2002].

#### 3.2.1. Gouge Thickness Reduction

As confining pressure is increased, the thickness of the gouge layer is expected to decrease as it compacts [*Bésuelle et al.*, 2000; *Bied et al.*, 2002; *Haied and Kondo*, 1997; *Skurtveit et al.*, 2013; *Uehara and Shimamoto*, 2004]. Such compaction is generally reflected in grain reorganization and porosity loss [*Mair et al.*, 2002;

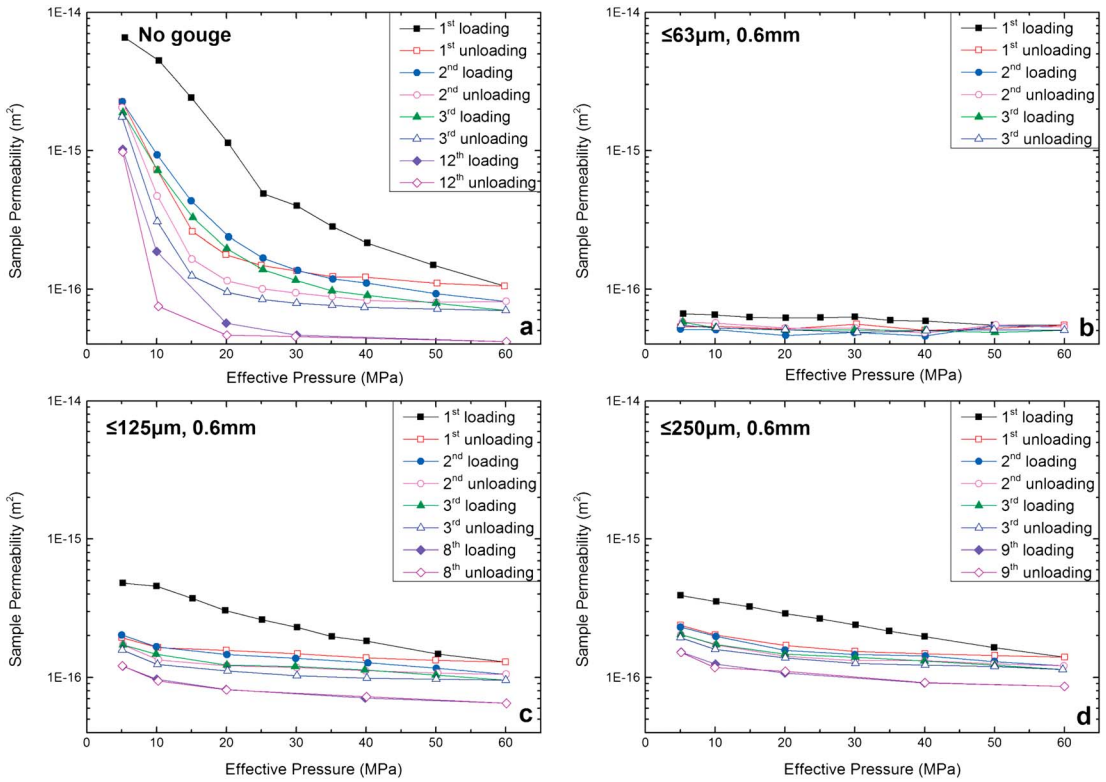


**Figure 5.** Effect of pressure cycling on permeability of sample with (a) no gouge, with 0.6 mm thickness of (b) ≤63 μm grain size gouge, (c) ≤125 μm grain size gouge, and (d) ≤250 μm grain size gouge.

*Zhang and Tullis*, 1998; *Zhang et al*., 2001]. We determined the reduction in gouge thickness by measuring the sample diameter perpendicular to the fracture (i.e., $D + T_G$ as in Figure 1d) after testing over different numbers of pressure cycles and comparing this with the initial value. In order to avoid any gouge particle breakage during depressurization, we reduced the pressure at a very low rate (less than 1 MPa $min^{-1}$). The results of our measurements are shown in Figure 6.

Figure 6a shows that for the same initial gouge thickness, the reduction in thickness after a single pressure cycle increases with the gouge particle size, which is consistent with the conclusions of *Haied and Kondo* [1997], *Bésuelle et al*. [2000], *Bied et al*. [2002], and *Skurtveit et al*. [2013]. Specifically, the thickness reduction in ≤63 μm gouge is only about 1.7%, while in the coarser-grained gouges of ≤125 μm, ≤250 μm, and ≤500 μm the reductions are 5.9%, 7.2%, and 10.6%, respectively. Following further pressure cycling to reach steady state permeability, the thickness of the ≤63 μm gouge shows no further reduction, while that of the ≤125 μm and the ≤250 μm gouges reduce further from 5.9% to 6.8% and from 7.2% to 8.3%, respectively. In Figure 6b, we show the dependence of gouge thickness reduction after a single pressure cycle on initial gouge thickness for two different grain sizes (≤63 μm and ≤250 μm). It is clear that the thickness reduction increases with increasing initial thickness but that it appears to approach a limiting value with increasing thickness. As expected from our earlier results (Figure 6a), the thickness reduction is significantly higher in the coarser-grained gouge.

### 3.2.2. Changes in PSD

The thickness changes we measured in our gouges may result not only from the rearrangement of gouge particles but also from their comminution, resulting in enhanced compaction [*Crawford et al*., 2008; *Guo and Morgan*, 2006; *Hardin*, 1985; *Mair and Abe*, 2011; *Mair et al*., 2002; *Sreenivasulu et al*., 2014; *Uehara and Shimamoto*, 2004]. If particle comminution is a significant process in our experiments, then we would expect this to be reflected in changes in the particle size distribution (PSD) of our gouges before and after pressurization [*Hardin*, 1985]. We therefore measured the PSD of all our gouges before testing and after different numbers of pressure cycles, as shown in Figure 7.

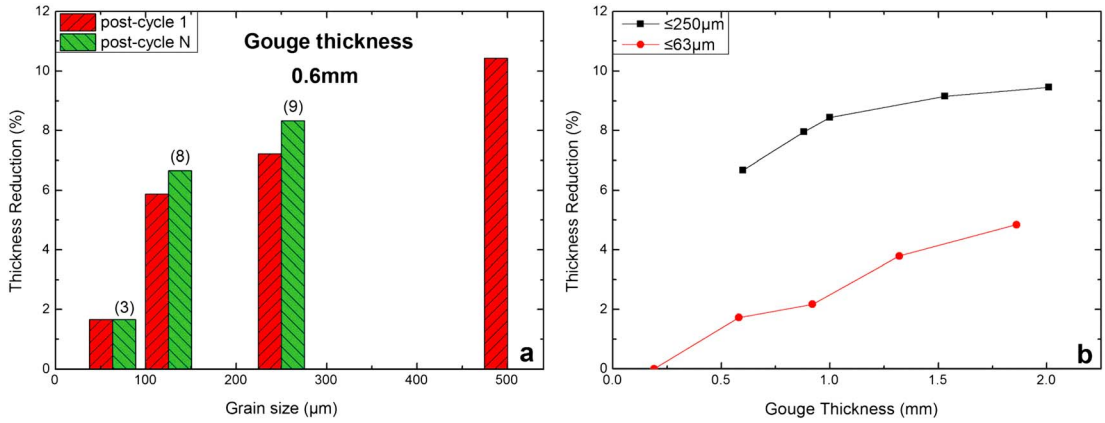


**Figure 6.** Gouge thickness reduction for (a) gouges of different grain sizes but the same initial thickness (0.6 mm here) after the first pressure cycle (postcycle 1) and after the number of pressure cycles required to reach steady state (postcycle *N*; number of cycles indicated on the Figure) and (b) gouges of different thicknesses and two grain sizes (indicated) after one pressure cycle.

Figure 7a shows that the PSD for the finer-grained gouges (≤63 μm, ≤108 μm, and ≤125 μm) both pretest and after different numbers of pressure cycles (indicated on the figure). All of these gouges have unimodal distributions, with the peak values being 20 μm (3.7%) for the ≤63 μm gouge, 40 μm (4.6%) for the ≤108 μm gouge, and 36 μm (3.8%) for the ≤125 μm gouge. After pressure cycling to 60 MPa, regardless of the number of cycles, there is no discernible change in the PSD of the ≤63 μm gouge. This suggests that all the measured thickness reductions for the finest-grained gouge was due solely to particle rearrangement in the gouge layer. There is a very small change in the PSD of the ≤125 μm gouge, just discernible for the largest particles in the PSD. This suggests the onset of a small amount of comminution at this grain size. By contrast, Figure 7b shows that the coarser-grained gouges (≤250 μm and ≤500 μm) have bimodal distributions, with the peak values being 30 μm (3.2%) and 178 μm (2.24%) for the ≤250 μm gouge and 35 μm (1.3%) and 450 μm (6.5%) for the ≤500 μm gouge. Figure 7b also shows that after pressure cycling, regardless of the number of cycles, there is a change in the PSD for all these gouges. In both cases, there is a reduction in the percentage of particles in the higher peak and an increase in the percentage of particles in the lower peak. For the ≤250 μm gouge the change is rather modest after one pressure cycle, but there is a significant reduction in the proportion of particles in the higher peak after nine pressure cycles (where the permeability reaches its minimum, steady state value). The change of PSD is most marked in the ≤500 μm gouge, where a significant decrease in the higher peak and a significant increase in the lower peak are observed after only a single pressure cycle. These observations suggest that the measured thickness reductions for these coarser gouges involve a significant amount of particle comminution in addition to particle rearrangement. The degree of particle comminution also appears to increase with increasing grain size.

## 4. Discussion

### 4.1. Effect of Gouge Characteristics on Permeability

#### 4.1.1. Comparison of Permeability With and Without Gouge

The introduction of a macrofracture into a previously intact rock sample with very low matrix permeability increases permeability dramatically, as shown in Figure 3. The addition of a gouge layer within the fracture decreases its permeability, but it still remains significantly higher than for the intact material (Figure 3). However, whether the fracture is unfilled or filled with gouge, the permeability always decreases as effective pressure is increased. These observations are entirely consistent with earlier studies which showed that both fracture aperture and fluid conductivity decrease sharply with depth (cf. pressure) due to elastic deformation of fracture surfaces and inelastic degradation of asperities [*Amiri Hossaini et al*., 2014; *Goodman*, 1976; *Kamali and Pournik*, 2016; *Nara et al*., 2011; *Patton*, 1966; *Pyrak-Nolte et al*., 1987; *Sagy et al*., 2007; *Walsh and Grosenbaugh*, 1965; *Zhang and Sanderson*, 1996]. The addition of a gouge layer within a fracture transfers the deformation from the fracture surfaces to the gouge particles [*Hoek and Bray*, 1981]. Gouge porosity therefore decreases progressively with increasing effective pressure due to elastic grain deformation,

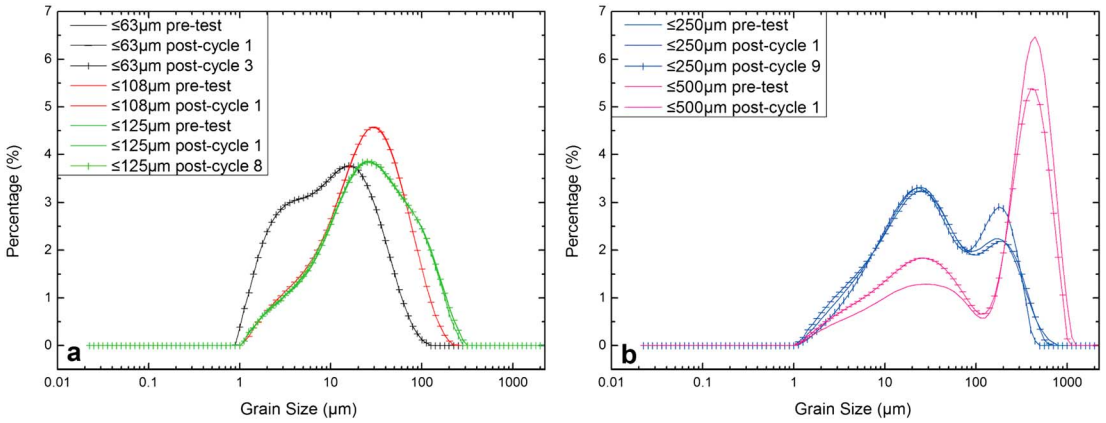


**Figure 7.** Changes of PSD of the same thickness (0.6 mm here) of various gouges before test (pretest—solid line), after single pressurization cycle (postcycle 1—solid line with dashes) and after pressure cycling (postcycle N—solid line with bars) for (a) ≤63 (black), ≤108 (red), and ≤125 μm (green) gouges and (b) ≤250 (blue) and ≤500 μm (pink) gouges.

inelastic grain rearrangement, and comminution [*Crawford et al*., 2008; *Faulkner and Rutter*, 1998, 2000; *Morrow et al*., 1984; *Morrow et al*., 1986; *Nara et al*., 2011].

Fractures are more compliant and close more easily at low stress due to the nonlinear relationship between fracture closure and normal stress [*Brown and Scholz*, 1985; *Goodman*, 1976; *Min et al*., 2004; *U.S. National Committee for Rock Mechanics*, 1996]. This is especially true for mated fractures, fractures with zero shear offset. Such fractures have very low aspect ratios [*Nara et al*., 2011], such that the fracture surfaces need only a low effective pressure to come into contact. Fractures become stiffer at higher effective pressures [*Goodman*, 1976], and higher normal stresses are required to reduce the fracture aperture further [*Goodman*, 1976; *U.S. National Committee for Rock Mechanics*, 1996]. We see all these features in our permeability measurements. While sample permeability depends on fracture aperture, the permeability of unfilled mated fractures here also shows a nonlinear correlation with normal pressure, as shown in Figure 3, which is consistent with the results of *Min et al*. [2004] and *Nara et al*. [2011].

The picture is very different for gouge-filled fractures. Gouge layers which have undergone the same pressure history exhibit only small reductions in thickness (hence, only small reductions in porosity) and only limited or no change in their PSD as shown in Figures 6a and 7. Gouge particles can fill the apertures of mated macrofractures easily, but the voids between the grains within the gouge are much more difficult to close, even under relatively high effective pressure. Therefore, we observe that gouge-filled samples exhibit lower permeabilities than unfilled macrofractures at low effective pressure and that the permeability gradient as a function of increasing effective pressure is much lower. Hence, the permeability of samples with gouge-filled fractures can exceed that of samples with unfilled fractures above a certain effective pressure (Figure 3). This observation has parallels with the observation of *Nara et al*. [2011] on samples containing both microfractures and macrofractures. They report that the easily closed macrofractures dominated the overall permeability at low effective pressure, while the harder-to-close microfractures increasingly dominated the permeability at higher effective pressure. We have also shown that the grain size of the gouge exerts a strong influence on the permeability. In particular, the finest-grained gouge (≤63 μm) behaves very differently from all the coarser gouges. Unlike the coarser-grained gouges, the fine-grained gouge shows no evidence of any grain comminution and only a minimal thickness reduction of 1.7% after a single pressurization/depressurization cycle (Figures 6a and 7). We suggest that the fracture aperture can be much more easily filled by the well-packed, fine-grained gouge (which contains particles of all sizes less than 63 μm) and that the void spaces between these small gouge particles are harder to close than the larger voids between the larger particles in the coarser-grained gouges. This explains not only why samples filled with ≤63 μm gouge have the lowest permeabilities (always lower than that of the unfilled fracture; Figure 3) but also why the permeability decreases the least with increasing effective pressure (Figure 3).

The relationship we observe between sample permeability and gouge grain size is not entirely consistent with previous observations by *Beard and Weyl* [1973] and *Morrow et al*. [1984], who found that permeability was proportional to gouge grain size, gouge porosity, and crack aperture. However, we attribute this

difference to the different grain size distribution of the gouges used in our experiments. Our gouges contained particles of all sizes below an upper limit, while those of these previous studies contained particles of uniform size. In our gouges, first, the finer grains within the distribution are able to infill the void spaces between the coarser grains and hence act to lower the permeability of the gouge [*Biegel et al*., 1989]. Second, we observe much stronger grain comminution and much larger reductions in gouge thickness following pressurization for gouges with increasing maximum grain size (Figures 6a and 7). These observations indicate that more inelastic compaction (and greater commensurate reduction in porosity) occurs in gouges containing coarser grains, in agreement with the conclusions of *Wong* [1990] and *Sreenivasulu et al*. [2014]. Third, we also need to consider the influence of gouge layer thickness. Figure 4b shows that the permeability of a sample containing a layer of coarse-grained gouge is sensitive to layer thickness and increases with increasing thickness (especially, up to 1.1 mm). This suggests that the influence on permeability of particle packing within a coarse-grained gouge layer may overwhelm the influence of the gouge grain size during a single pressurization cycle. In turn, this may explain why fractures filled with a gouge layer of the same initial thickness, but different particle sizes (discounting the finest gouge) exhibit very similar permeabilities over the whole pressure range, as shown in Figure 3.

#### 4.1.2. Effect of Pressure Cycling on Permeability

While this is the first systematic study of how the permeability of gouge-filled macrofractures respond to stress history during pressure cycling, several complementary studies have made somewhat similar measurements on intact crystalline rock [*Morrow et al*., 1986] and natural fault gouge [*Faulkner and Rutter*, 1998, 2000]. The permeability of intact crystalline rocks was found to decrease on pressure cycling but then found to recover its initial value after an extended period following depressurization, regardless of the applied confining pressure [*Morrow et al*., 1986]. Such an elastic behavior suggests both elastic hysteresis due to reversible deformation of preexisting microcracks, and time-dependent relaxation hindered by friction at contacts between the rough crack surfaces [*Walsh*, 1965], such that they are unable to reopen immediately upon pressure release [*Morrow et al*., 1986]. Significant permeability hysteresis was observed in fault gouge during the initial pressure cycle [*Faulkner and Rutter*, 1998, 2000; *Morrow et al*., 1984], but this gradually reduced with increasing cycling number until a constant value was achieved for any given effective pressure after about 10 cycles [*Faulkner and Rutter*, 2000]. However, the permeability of the gouge neither decreased nor increased during extended hold times between pressure cycles, suggesting that the permeability hysteresis arose primarily from irreversible or inelastic compaction caused by the rearrangement of phyllosilicate particles, and without any appreciable time-dependent elastic compaction [*Faulkner and Rutter*, 1998, 2000].

Reversible deformation of the macrofractured sample and slow stress relaxation in comparison to the test duration can likely explain part of permeability hysteresis of the unfilled sample, e.g., the elastic hysteresis loop at steady state (the 12th cycle here) observed in Figure 5a. However, both the permanent permeability hysteresis (or inelastic hysteresis) in each cycle and the observation that the largest reduction in permeability occurs after the first cycle, with all subsequent cycles having decreasing magnitude of hysteresis until no further change is seen with cycles, cannot be explained by the conclusions drawn by *Morrow et al*. [1986] and *Faulkner and Rutter* [1998, 2000]. Rock fractures consist of rough surfaces with asperities at the macroscopic scale (primary asperities) and microscopic scale (secondary asperities) [*Lee et al*., 2001; *Patton*, 1966]. During confining pressure cycling, these rough surfaces have cyclic loads applied on small asperities interacting with each other on either side of the experimental fracture. Stress at such small asperities can be high and where asperity contacts are small, stress can exceed the local strength of the rock leading to the elastic/inelastic deformation of the asperities [*Pyrak-Nolte et al*., 1987; *Scholz and Hickman*, 1983]. Asperity deformation with cyclic pressurization will result in a change in the average macrofracture aperture, which has a significant effect on permeability. Elastic deformation occurs on both primary and secondary asperities where normal stress is applied (i.e., no shear stress), while inelastic deformation occurs at secondary asperities during pressure loading, which means only elastic deformation occurs during pressure unloading [*Matsuki et al*., 2008; *Pyrak-Nolte et al*., 1987]. The variation in asperity deformation during unloading and loading processes and the slow strain relaxation of asperities compared to the duration of tests lead to the occurrence of hysteresis in fracture opening and closure [*Goodman*, 1976; *Matsuki et al*., 2008; *Morrow et al*., 1986]. However, the irreversible part of the hysteresis that is caused by the degradation of secondary asperities is not equal for each load cycle, suggesting that the majority of secondary asperities were deformed during the first loading cycle, and the amount of asperity deformation decreases with each subsequent cycle until no further change

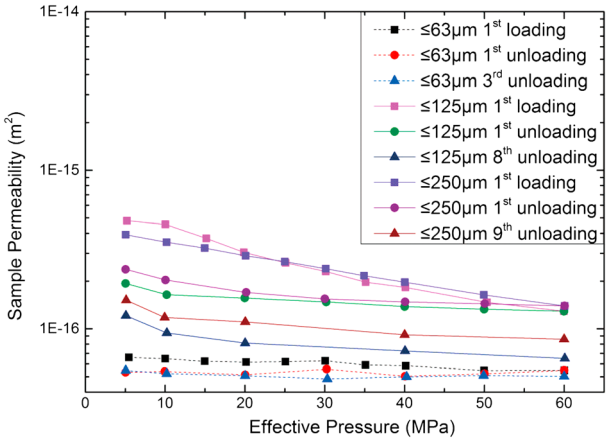


**Figure 8.** Comparison of the effect of pressure cycling on the same thickness (0.6 mm here) of gouges with coarse grains (≤125 μm and ≤250 μm here) with that of fine-grained gouge (≤63 μm, dashed line) as the baseline. Square, circle, and triangle symbols represent data after the first loading process, the first unloading process, and the final unloading process when they reach steady status, respectively.

is seen [*Bernabe*, 1987; *Lee et al*., 2001; *Scholz and Hickman*, 1983]. It is likely that the smallest asperities with high stress concentrations break first, and once the asperity is deformed, the contact area is larger and below the contact strength. The reversible part of the hysteresis due to the elastic deformation of asperities in each cycle becomes more apparent as the secondary asperities are degraded with increasing pressure cycles, until eventually only the reversible hysteresis loop is observed as steady state is reached, similar to the hysteresis loops described by *Walsh* [1965] and *Tutuncu et al*. [1997]. Due to the nonlinear relationship between fracture closure and normal stress [*Brown and Scholz*, 1985; *Goodman*, 1976; *Min et al*., 2004; *U.S. National Committee for Rock Mechanics*, 1996], this hysteresis is more appreciable at lower pressures. It is clear therefore that there is a subtle contribution of both elastic and inelastic processes occurring that contribute to the permeability hysteresis observed in Figure 5a.

The permeability hysteresis observed in Figures 5b–5d on our gouge-filled samples agree with the results of *Faulkner and Rutter* [1998, 2000] on natural fault gouge showing that the permeability reduction of gouge is primarily the result of irreversible reshuffling of gouge grains. However, our data do show some differences. By comparing the permeability results of unfilled and filled samples in Figure 5, we found some of the results for the unfilled sample also hold true for gouge-filled fractures. While the microscale mechanisms are different, the addition of a gouge layer in the fracture transfers the deformation from asperities on the fracture wall to the gouge grains [*Amiri Hossaini et al*., 2014; *Hoek and Bray*, 1981]. From Figures 5b–5d, the irreversible permeability reduction hysteresis was also only observed during the increasing pressure stage of the cycles before it disappears, suggesting that the inelastic deformation of gouge caused by grain rearrangement and/or comminution [*Crawford et al*., 2008; *Faulkner and Rutter*, 1998, 2000; *Morrow et al*., 1984; *Morrow et al*., 1986; *Nara et al*., 2011] occurs only under increasing pressure part of the cycle. Thus, the significant reduction in permeability of the fault gouge occurred after the first loading process rather than after initial pressure cycle, as shown by *Morrow et al*. [1984] and *Faulkner and Rutter* [1998, 2000]. The thickness reduction (inelastic deformation) of gouge after the first loading cycle (Figure 6) accounts for the majority of the reduction in gouge thickness achieved after the steady state is reached, explaining why the significant permeability hysteresis is observed after the first cycle and decreasing with increasing cyclic loading. The changes in PSD (Figure 7) during the first loading process of the finer grained gouge indicates that it is primarily grain rearrangement of gouge that caused the inelastic deformation of gouge and permeability reduction, but for gouge containing grains coarser than 125 μm, some grain comminution was also observed. Successive pressure cycles show that no further changes of either thickness or PSD of the gouge was observed for the finest grained material. This explains why the ≤63 μm gouge reached a steady state immediately after the first loading cycle. By contrast, further PSD changes were observed for the larger particles in gouges containing coarser grains, indicating that particle comminution is more prevalent for larger grains. This explains why further permeability hysteresis in Figures 5c and 5d and further thickness reduction in Figure 6a were observed for gouges containing larger grains before they reached steady state.

As discussed in section 3.1.1, after the initial pressure loading, similar permeabilities were measured in samples filled with coarser grain gouges, for instance, ≤125 μm and ≤250 μm gouges here (Figure 8). It might be expected that after pressure cycling, the sample filled with ≤250 μm gouge would have a lower permeability than that filled with ≤125 μm gouge, as it would experience larger amounts of grain comminution and a larger porosity loss than that of the ≤125 μm gouge, as showed in Figures 6a and 7. In fact, the opposite

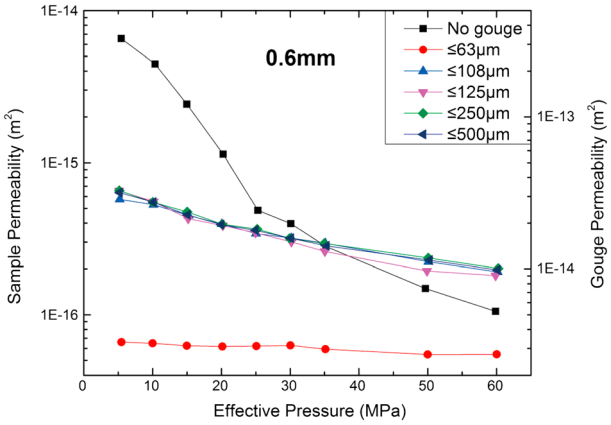


**Figure 9.** The comparison of sample permeability and gouge permeability of macrofractured sample with no gouge and with the same thickness (0.6 mm) of different grain sizes gouge layers under elevated effective pressure.

occurs, and even from the first unloading cycle, the permeability of sample filled with ≤250 μm gouge is greater than that of sample filled with ≤125 μm gouge, as the solid lines with circles show in Figure 8. This difference becomes greater with increased cycling until the permeability reaches a minimum value as steady state is reached. This final permeability is greater than that of the ≤63 μm gouge (lines with circles in Figure 8), which indicates an increasing influence of denser grain packing on permeability. The suggestion that sample permeability is proportional to its grain size [*Beard and Weyl*, 1973; *Morrow et al*., 1984] should be also correct for gouges with a wider range of grain sizes, as long as they are densely packed.

Thus, we can conclude that independent of sample type, i.e., intact, fractured (both microfractured and macrofractured ones) or gouge filled, the stress history of the material must be specified in order to fully describe the permeability dependence on effective pressure, in agreement with the results of *Morrow et al*. [1986] on intact samples.

#### 4.1.3. Comparison of Sample Permeability and Gouge Permeability

As noted earlier, gouge thickness is considered to be an important factor influencing the sealing capacity of faults. However, very few previous studies have been conducted to measure the effect of gouge thickness on permeability.

The lowest permeability measured for any of our samples with gouge-filled fractures was approximately $6\times10^{-17}$ m$^2$ (for ≤63 μm gouge; Figure 3), which is more than 3 orders of magnitude higher than that of the intact basalt [*Nara et al*., 2011]. Therefore, fluid flow through the intact basalt matrix is essentially negligible compared with flow through the gouge layer in our macrofractured samples. Thus, the fluid flow through the gouge is essentially equal to the fluid flow through the whole sample. Using this assumption, we can compare directly the sample permeability $\boldsymbol{k}$ with the gouge permeability $\boldsymbol{k_g}$ simply by comparing their cross-sectional areas.

Hence,

$$\boldsymbol{k} = \boldsymbol{k_g}[(\boldsymbol{D}.\boldsymbol{t})/(\boldsymbol{A}+\boldsymbol{D}.\boldsymbol{t})] \quad (2)$$

where $\boldsymbol{A}$ is the cross-sectional area of the intact sample, $\boldsymbol{D}$ is the sample diameter, and $\boldsymbol{t}$ is the thickness of the gouge layer. For samples with gouge layers of the same thickness but of different grains size, the sample permeability is then directly proportional to the permeability of the gouge layer. For a gouge layer thickness of 0.6 mm, as shown in Figure 3, the ratio $\boldsymbol{k_g/k}$ is about 50. Figure 9 shows the comparison between sample permeability and gouge permeability for the data of Figure 3.

We can also use the relationship (2) to analyze the influence of layer thickness on gouge permeability. We note from Figure 4 that sample permeability increases with increasing gouge layer thickness (especially for the coarser-grained gouge). However, it is also clear that the proportional increase in sample permeability is smaller than the proportional increase in thickness. The data of Figure 4 are therefore recalculated and replotted as gouge permeabilities in Figure 10.

Figure 10 shows clearly that gouge permeability actually decreases with increasing layer thickness for both the ≤63 μm and ≤250 μm gouges. This observation may seem counterintuitive but is entirely supported by the complementary observation that the percentage reduction in gouge layer thickness on pressurization increases with increasing thickness (see the data of Figure 6b). Reduction in layer thickness implies a reduction in porosity which, in turn, is entirely compatible with a reduction in permeability. This observation is also

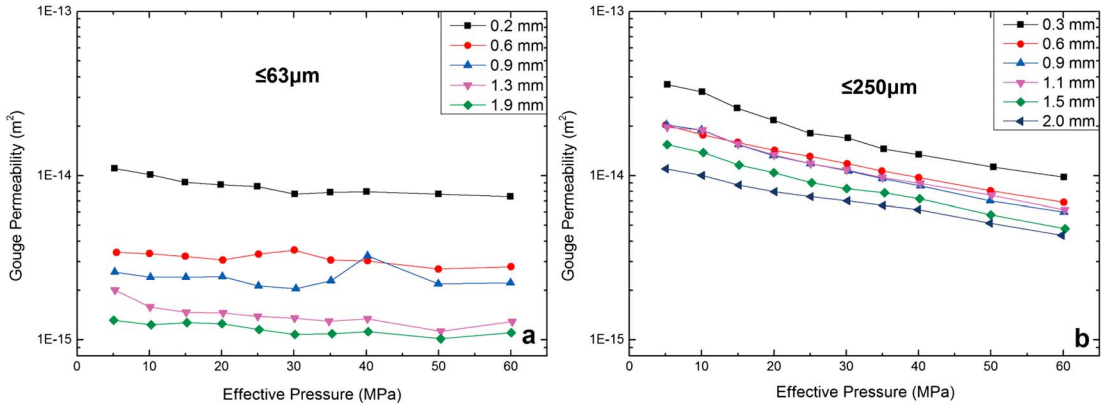


**Figure 10.** Permeability of sample and gouge with growing thicknesses under increasing effective pressure for (a) ≤63 μm gouge and (b) ≤250 μm gouge.

in agreement with results reported by *Aharonov and Sparks* [1999] that greater compaction occurs in thicker granular layers due to stronger internal grain rearrangement and comminution. Figure 10 also shows that the permeability decrease in fine-grained gouge is significantly more sensitive to thickness change than that in coarse-grained gouge, even though there is significantly less reduction in thickness of fine-grained gouge when it is pressurized (see Figure 6b). Therefore, we suggest that overall sample permeability depends both on gouge thickness and on gouge permeability which, in turn, decreases with thickness and is sensitive to grain size.

### 4.2. Implications for the Permeability of Natural Fractures

In nature, fractures can be either open (e.g., joints) or gouge filled (e.g., shear faults). The presence of gouge in fractures has a major influence on their permeability [e.g., *Caine et al*., 1996]. Our results suggest that at shallow depths, unfilled fractures or joints will have higher permeability than gouge-filled fractures. However, there is a crossover depth at which this changes and unfilled fractures such as well-mated joints close sufficiently for their permeability to become lower than that of gouge-filled fractures. This is because the distribution of particle sizes in the gouge, commonly observed to be fractal [*Sammis et al*., 1986], is able to maintain some open porosity which continues to provide pathways for fluid flow even at greater depth. This has potentially important implications for fluid flow through jointed rocks masses which have commonly been thought to act as conduits for high fluid flux, since at greater depths their permeability may be lower than that of rock masses characterized by gouge filled shear fractures.

Many natural fractures are also subject to temporal variations in effective pressure, whether it be changes in fault normal stress or coseismic changes in fluid pressure. Such cyclic loading can alter the particle size distribution of fracture filling gouge through changes in grain packing and particle comminution, and this will in turn change the permeability and hence the crossover depth. Furthermore, it is well known that particle size distribution evolves with shear displacement, but our results show that this can also be achieved by the cycling of effective pressure without any need for shear displacement. This observation has implications for both natural cyclic loading cases, but, in particular, for anthropogenic processes involving the extraction or injection of fluids into crustal rocks.

## 5. Conclusions

Progressive decrease in aperture of unfilled fractures and in porosity of gouge in filled fractures with increasing effective pressure results in reduction of sample permeability. However, the permeability reduces much faster in unfilled mated samples due to the nonlinear relationship between fracture closure and normal stress. The presence of a gouge layer generally lowers the permeability of fractures at low effective pressure. However, where fractures are filled with coarse-grained gouge, the sample permeability can become higher than the fracture permeability above some critical pressure due to the propping open of the fracture by coarse grains and the difficulty of closing voids between grains.

The permeability of gouge-filled samples shows a positive relationship with gouge grain size. The results might be not always the case if the gouge packing experiences only a single pressurization process, as inelastic compaction might overwhelm the influence of grain size on permeability. This is especially true for gouge with coarse grains. Due to the greatly reduced inelastic compaction of gouge, grain size of gouge becomes a primary control on sample permeability with further and greater pressure loading. Thus, to discuss the effect of grain size, the stress history of gouge must be specified.

Pressure cycling has a big impact on permeability evolution of both unfilled and filled samples. During pressure cycles, both elastic and inelastic deformation of sample materials occur to adjust the permeability of sample, but inelastic deformation of sample materials only happens during loading, which causes the permanent permeability loss of sample. The inelastic deformation of sample materials is much stronger during the first loading cycle than that of the following cycles. But due to the slow strain relaxation of asperities on fracture surfaces compared to the duration of tests, reversible hysteresis is still observed as the steady status is reached, while because the deformation of gouge-filled samples mainly rely on the rearrangement or comminution of grains in the gouge, which cause limited elastic deformation, no reversible hysteresis exists. Pressure cycling also influences the deformation mechanism of gouge. During the first pressure cycle the grain rearrangement of gouge accounts for the most inelastic deformation, but with further cycles, grain comminution contributes in gouge containing coarse grains. The effect of grain comminution is stronger with increasing grain size.

Generally, sample permeability depends on both gouge thickness and its permeability, which decreases with gouge thickness due to increased porosity loss under the same experimental conditions. There is no unified correlation between sample permeability and gouge thickness. Gouge containing coarse grains is less sensitive to thickness change than that of fine-grained gouge. We observe a positive correlation between sample permeability and its thickness, while for fine-grained gouge, their relationship is still unclear; more work needs to be done in the future.

**Acknowledgments**

We would like to thank John Bowles, Neil Hughes, Steve Boon, and Ian Patmore from University College London for their help and advice with sample preparation and the experimental program. Pamela Perez is thanked for help with experiments, and John Browning for his comments on an early version of this manuscript. T.M.M. and P.M. acknowledge funding from NERC grant NE/N002938/1. Data for this paper are available by contacting the corresponding author at guangzengwang@gmail.com.

## References

Aharonov, E., and D. Sparks (1999), Rigidity phase transition in granular packings, *Phys. Rev.*, *60*(6), 6890–6896.

Amiri Hossaini, K., N. Babanouri, and S. Karimi Nasab (2014), The influence of asperity deformability on the mechanical behavior of rock joints, *Int. J. Rock Mech. Min. Sci.*, *70*, 154–161, doi:10.1016/j.ijrmms.2014.04.009.

An, L. J., and C. G. Sammis (1994), Particle size distribution of cataclastic fault materials from Southern California: A 3-D study, *Pure Appl. Geophys.*, *143*(1), 203–227.

Anthony, J. L., and C. Marone (2005), Influence of particle characteristics on granular friction, *J. Geophys. Res.*, *110*, B08409, doi:10.1029/2004JB003399.

Aydin, A. (1978), Small faults formed as deformation bands in sandstone, *Pure Appl. Geophys.*, *116*(4), 913–930.

Beard, D. C., and P. K. Weyl (1973), Influence of texture on porosity and permeability of unconsolidated sand, *AAPG Bull.*, *57*(2), 349–369.

Berkowitz, B. (2002), Characterizing flow and transport in fractured geological media: A review, *Comput. Commun. ISCC Proceedings Third IEEE Symp.*, *25*(8–12), 861–884.

Bernabe, Y. (1987), The effective pressure law for permeability during pore pressure and confining pressure cycling of several crystalline rocks, *J. Geophys. Res.*, *92*(B1), 649–657, doi:10.1029/JB092iB01p00649.

Bésuelle, P., J. Desrues, and S. Raynaud (2000), Experimental characterisation of the localisation phenomenon inside a Vosges sandstone in a triaxial cell, *Int. J. Rock Mech. Min. Sci.*, *37*(8), 1223–1237.

Bied, A. E., J. Sulem, and F. Martineau (2002), Microstructure of shear zones in Fontainebleau sandstone, *Int. J. Rock Mech. Min. Sci.*, *39*(7), 917–932.

Biegel, R. L., C. G. Sammis, and J. H. Dieterich (1989), The frictional properties of a simulated gouge having a fractal particle distribution, *J. Struct. Geol.*, *11*(7), 827–846.

Brown, S. R., and C. H. Scholz (1985), Closure of random elastic surfaces in contact, *J. Geophys. Res.*, *90*(90), 5531–5545, doi:10.1029/JB090iB07p05531.

Caine, J. S., J. P. Evans, and C. B. Forster (1996), Fault zone architecture and permeability structure, *Geology*, *24*(11), 1025–1028.

Cladouhos, T. T. (1999), Shape preferred orientations of survivor grains in fault gouge, *J. Struct. Geol.*, *21*(4), 419–436.

Crawford, B. R., D. R. Faulkner, and E. H. Rutter (2008), Strength, porosity, and permeability development during hydrostatic and shear loading of synthetic quartz-clay fault gouge, *J. Geophys. Res.*, *113*, B03207, doi:10.1029/2006JB004634.

Deming, D. (1994), Factors necessary to define a pressure seal, *AAPG Bull.*, *78*(6), 1005–1009.

Eccles, D., P. R. Sammonds, and O. C. Clint (2005), Laboratory studies of electrical potential during rock failure, *Int. J. Rock Mech. Min. Sci.*, *42*(7), 933–949.

Faulkner, D. R., and E. H. Rutter (1998), The gas permeability of clay-bearing fault gouge at 20°C, *Geol. Soc. Lond. Spec. Publ.*, *147*(1), 147–156.

Faulkner, D. R., and E. H. Rutter (2000), Comparisons of water and argon permeability in natural clay-bearing fault gouge under high pressure at 20°C, *J. Geophys. Res.*, *105*(B7), 16,415–16,426, doi:10.1029/2000JB900134.

Goodman, R. E. (1976), *Methods of Geological Engineering Discontinuous Rock*, West Publishing Co, St. Paul.

Gueguen, Y., T. Chelidze, and M. L. Ravalec (1997), Microstructures, percolation thresholds, and rock physical properties, *Tectonophysics*, *279*(1), 23–35.

Guo, Y., and J. K. Morgan (2006), The frictional and micromechanical effects of grain comminution in fault gouge from distinct element simulations, *J. Geophys. Res.*, *111*, B12406, doi:10.1029/2005JB004049.

Hadley, K. (1976), The effect of cyclic stress on dilatancy: Another look, *J. Geophys. Res.*, *81*(14), 2471–2474, doi:10.1029/JB081i014p02471.
Haied, A., and D. Kondo (1997), Strain localization in Fontainebleau sandstone: Macroscopic and microscopic investigations, *Int. J. Rock Mech. Min. Sci.*, *34*(3–4), 161–173.
Hardin, B. O. (1985), Crushing of soil particles, *J. Geotech. Eng.*, *111*(10), 1177–1192.
Hoek, E., and J. Bray (1981), *Rock Slope Engineering*, 4th ed., CRC Press, Boca Raton, Fla.
Kamali, A., and M. Pournik (2016), Fracture closure and conductivity decline modeling—Application in unpropped and acid etched fractures, *J. Unconv. Oil Gas Resour.*, *14*, 44–55, doi:10.1016/j.juogr.2016.02.001.
Kendall, K. (1978), The impossibility of comminuting small particles by compression, *Nature*, *272*(5655), 710–711.
Krumbein, W. C., and E. J. Aberdeen (1937), The sediments of Barataria Bay [Louisiana], *J. Sediment. Res.*, *7*(1), 3–17.
Lang, B., and R. Anthony (2004), Numerical simulation of comminution in granular materials with an application to fault gouge evolution.
Lee, H. S., Y. J. Park, T. F. Cho, and K. H. You (2001), Influence of asperity degradation on the mechanical behavior of rough rock joints under cyclic shear loading, *Int. J. Rock Mech. Min. Sci.*, *38*(7), 967–980, doi:10.1016/S1365-1609(01)00060-0.
Ma, J. (2015), Review of permeability evolution model for fractured porous media, *J. Rock Mech. Geotech. Eng.*, *7*(3), 351–357, doi:10.1016/j.jrmge.2014.12.003.
Mair, K., and S. Abe (2011), Breaking up: Comminution mechanisms in sheared simulated fault gouge, *Pure Appl. Geophys.*, *168*(12), 2277–2288.
Mair, K., S. Elphick, and I. Main (2002), Influence of confining pressure on the mechanical and structural evolution of laboratory deformation bands, *Geophys. Res. Lett.*, *29*(10, 1410), doi:10.1029/2001GL013964.
Matsuki, K., E. Q. Wang, A. A. Giwelli, and K. Sakaguchi (2008), Estimation of closure of a fracture under normal stress based on aperture data, *Int. J. Rock Mech. Min. Sci.*, *45*(2), 194–209, doi:10.1016/j.ijrmms.2007.04.009.
Michibayashi, K. (1996), The role of intragranular fracturing on grain size reduction in feldspar during mylonitization, *J. Struct. Geol.*, *18*(1), 17–25.
Min, K. B., J. Rutqvist, C. F. Tsang, and L. Jing (2004), Stress-dependent permeability of fractured rock masses: A numerical study, *Int. J. Rock Mech. Min. Sci.*, *41*(7), 1191–1210.
Morrow, C. A., L. Q. Shi, and J. D. Byerlee (1981), Permeability and strength of San Andreas Fault gouge under high pressure, *Geophys. Res. Lett.*, *8*(8), 325–328, doi:10.1029/GL008i004p00325.
Morrow, C. A., L. Q. Shi, and J. D. Byerlee (1984), Permeability of fault gouge under confining pressure and shear stress, *J. Geophys. Res.*, *89*(B5), 3193–3200, doi:10.1029/JB089iB05p03193.
Morrow, C. A., B. C. Zhang, and J. D. Byerlee (1986), Effective pressure law for permeability of westerly granite under cyclic loading, *J. Geophys. Res.*, *91*(B3), 3870–3876, doi:10.1029/JB091iB03p03870.
Nara, Y., P. Meredith, T. Yoneda, and K. Kaneko (2011), Influence of macro-fractures and micro-fractures on permeability and elastic wave velocities in basalt at elevated pressure, *Tectonophysics*, *503*(1–2), 52–59.
Nara, Y., P. Meredith, and T. Mitchell (2013), Influence of macro-fractures and fault gouge on permeability in basalt (abstract) paper presented at Geophysical Research Abstracts.
Patton, F. D. (1966), Multiple modes of shear failure in rock paper presented at Proceeding of the1st Congress of International Society of Rock Mechanics.
Pyrak-Nolte, L. J., L. R. Myer, N. G. W. Cook, and P. A. Witherspoon (1987), Hydraulic and mechanical properties of natural fractures in low permeable rock Proc. 6th Int. Cong. Rock Mech.
Rutter, E. H., R. H. Maddock, S. H. Hall, and S. H. White (1986), Comparative microstructures of natural and experimentally produced clay-bearing fault gouges, *Pure Appl. Geophys.*, *124*(1–2), 3–30.
Sagy, A., E. E. Brodsky, and G. J. Axen (2007), Evolution of fault-surface roughness with slip, *Geology*, *35*(3), 283–286, doi:10.1130/g23235a.1.
Sammis, C. G., H. O. Robert, J. L. Anderson, M. Banerdt, and P. White (1986), Self-similar cataclasis in the formation of fault gouge, *Pure. Appl. Geophys.*, *124*(1), 53–78, doi:10.1007/bf00875719.
Scholz, C. H., and S. H. Hickman (1983), Hysteresis in the closure of a nominally flat crack, *J. Geophys. Res.*, *88*(B8), 6501–6504, doi:10.1029/JB088iB08p06501.
Scholz, C. H., and T. A. Koczynski (1979), Dilatancy anisotropy and the response of rock to large cyclic loads, *J. Geophys. Res.*, *84*(B10), 5525–5534, doi:10.1029/JB084iB10p05525.
Screaton, E. J., D. R. Wuthrich, and S. J. Dreiss (1990), Permeabilities, fluid pressures, and flow rates in the Barbados Ridge Complex, *J. Geophys. Res.*, *95*(B6), 8997–9007, doi:10.1029/JB095iB06p08997.
Skurtveit, E., A. Torabi, R. H. Gabrielsen, and M. D. Zoback (2013), Experimental investigation of deformation mechanisms during shear-enhanced compaction in poorly lithified sandstone and sand, *J. Geophys. Res. Solid Earth*, *118*, 4083–4100, doi:10.1002/jgrb.50342.
Sreenivasulu, C., T. Sravani, M. Seshalalitha, and R. Pavani (2014), Influence of coarse fraction on compaction characteristics and cbr strength a fine grained soil, *Int. J. Adv. Eng. Technol.*, *7*(4), 1217–1226.
Tutuncu, A. N., A. L. Podio, and M. M. Sharma (1997), Nonlinear viscoelastic behavior of sedimentary rocks, Part II: Hysteresis effects and influence of type of fluid on elastic moduli, *Leading Edge*, *63*(1), 1895–1203.
Uehara, S., and T. Shimamoto (2004), Gas permeability evolution of cataclasite and fault gouge in triaxial compression and implications for changes in fault-zone permeability structure through the earthquake cycle, *Tectonophysics*, *378*(3–4), 183–195.
US National Committee for Rock Mechanics (1996), *Rock Fractures and Fluid Flow*, National Academy Press, Washington, DC.
Walsh, J. B. (1965), The effect of cracks on the uniaxial elastic compression of rocks, *J. Geophys. Res.*, *70*(2), 399–412, doi:10.1029/JZ070i002p00399.
Walsh, J. B. (1981), Effect of pore pressure and confining pressure on fracture permeability, *Int. J. Rock Mech. Min. Sci. Geomech. Abstr.*, *18*(5), 429–435.
Walsh, J. B., and M. A. Grosenbaugh (1965), A new model for analyzing the effect of fractures on compressibility, *Class. Rev.*, *18*(34), 10,669–10,676.
Watts, N. L. (1987), Theoretical aspects of cap-rock and fault seals for single- and two-phase hydrocarbon columns, *Mar. Pet. Geol.*, *4*(4), 274–307.
Wissler, T. M., and G. Simmons (1985), The physical properties of a set of sandstones—Part II. Permanent and elastic strains during hydrostatic compression to 200 MPa, *Int. J. Rock Mech. Min. Sci. Geomech. Abstr.*, *22*(6), 393–406.
Wong, T. F. (1990), Mechanical compaction and the brittle-ductile transition in porous sandstones, *Geol. Soc. London Spec. Publ.*, *54*, 111–122.
Zhang, S., and T. E. Tullis (1998), The effect of fault slip on permeability and permeability anisotropy in quartz gouge, *Tectonophysics*, *295*(1), 41–52.

Zhang, S., T. E. Tullis, and V. J. Scruggs (1999), Permeability anisotropy and pressure dependency of permeability in experimentally sheared gouge materials, *J. Struct. Geol.*, *21*(7), 795–806.

Zhang, S., T. E. Tullis, and V. J. Scruggs (2001), Implications of permeability and its anisotropy in a mica gouge for pore pressures in fault zones, *Tectonophysics*, *335*(1), 37–50.

Zhang, X., and D. J. Sanderson (1996), Effects of stress on the two-dimensional permeability tensor of natural fracture networks, *Geophys. J. Int.*, *125*(3), 912–924.

Zoback, M. D., and J. D. Byerlee (1975), The effect of cyclic differential stress on dilatancy in Westerly granite under uniaxial and triaxial conditions, *J. Geophys. Res.*, *80*(11), 1526–1530, doi:10.1029/JB080i011p01526.